LONGITUDINAL HADRONIC FLOW AT RHIC IN EXTENDED STATISTICAL THERMAL MODEL AND RESONANCE DECAY EFFECTS

Saeed Uddin[†], Jan Shabir Ahmad[‡], Majhar Ali
Waseem Bashir, Riyaz Ahmad Bhat

Department of Physics, Jamia Millia Islamia Central University
New Delhi 110025, India

M. Farooq Mir

Department of Physics, University of Kashmir, Srinagar, J&K, India

(Received July 5, 2010; revised version received August 15, 2010)

We use a recently proposed extended statistical thermal model to describe various hadron *rapidity spectra* at the highest RHIC energy (200 GeV/A). The model assumes the formation of hot and dense regions (fireballs) moving along the beam axis with increasing rapidities y_{FB}. This model has been earlier used to describe the net proton *i.e.* p–$\bar{p}$, ratio $\bar{p}/p$ and the pion rapidity spectra. In this paper we have attempted to show that in addition to these quantities, this model can also successfully describe the *individual* rapidity spectra of protons, antiprotons, Kaons, antiKaons, pions, the ratios $\bar{\Lambda}/\Lambda$ and $\bar{\Xi}/\Xi$. We have also investigated the effect of the inclusion of the resonance decay contributions on the rapidity spectra of various hadrons. We have found that the resonance decay contributions *do not modify* the rapidity spectra of hadrons to any significant extent, in the presence of longitudinal flow. The experimental data set on p, $\bar{p}$, K^+, K^- and π provided by BRAHMS Collaboration at the highest energy of Relativistic Heavy Ion Collider, $\sqrt{S_{NN}} = 200$ GeV are used. The theoretical results also fit quite well with mid-rapidity data (for $|y| < 1$) of the $\bar{\Lambda}/\Lambda$ and the $\bar{\Xi}/\Xi$ ratios available (from STAR). We have used single set of model parameters including single value of the temperature parameter T for all the regions of the hot and dense matter formed (fireballs). The chemical potentials of the different regions in the model are, however, assumed to be dependent on the fireball's or regions's rapidity, y_{FB}. We have also imposed the criteria of exact strangeness conservation in each region separately. We also discuss what can be learned about the nuclear transparency effect at the highest RHIC energy from the net proton rapidity distribution.

PACS numbers: 24.10.Pa, 24.10.–I, 25.75–q, 25.75.Dw

[†] saeed_jmi@yahoo.co.in
[‡] On leave of deputation from Department of Physics, Amar Singh College, Srinagar, J&K, India.

1. Introduction

The yields of baryons and antibaryons are an important indicator of the multi-particle production phenomenon in the ultra-relativistic nucleus–nucleus collisions. Great amount of experimental data have been obtained in such experiments ranging from the AGS energies to the RHIC. The study of ultra-relativistic nuclear collisions allows us to learn how baryon numbers initially carried by the nucleons only, before the nuclear collision, are distributed in the final state [1] at the thermo-chemical freeze-out after the collision. It is possible to obtain important information about the energy loss of the colliding nuclei by analyzing the rapidity dependence of the p and $\bar{p}$ production. The measurement of the *net* proton rapidity density distribution (*i.e.* p–$\bar{p}$) in such experiments can throw light on the collision scenario, *viz.* the extent of nuclear stopping/transparency, the subsequent formation of the fireball(s) and the degree of thermo-chemical equilibration of various hadronic resonances. The net proton flow at the AGS energy showed a peak at midrapidity, while at the top SPS energy ($\sqrt{S_{NN}} \approx 17.2$ GeV) the distribution started showing a minimum at midrapidity. The SPS data at different energies (20, 30, 40, 80, 158 GeV/A) show [1] that at midrapidity the p–$\bar{p}$ yield decreases gradually with increasing energy. This implies that at SPS energies the nuclear collisions start exhibiting some transparency. Hence, this new property, namely the extended longitudinal scaling in the rapidity distributions has emerged [1–5]. This has been observed in pp collisions at the highest RHIC energies as well as ultra-relativistic nuclear collisions [5,6]. Data from the BRAHMS Collaboration [7] clearly show that the antiproton to proton ratio shows a maximum at mid rapidity and gradually decreases towards larger rapidities, whereas the net proton rapidity density distribution shows a broad minimum, spanning about ± 1 unit around mid-rapidity region of dN/dy spectra. It was, therefore, conjectured [7] that at RHIC energies the collisions are (at least partially) transparent. Though the midrapidity region at RHIC is not yet totally baryon free, however, a transition from a baryon dominated system at lower energies to an *almost* baryon free system in the midrapidity at RHIC can be observed. An interesting analysis by Stiles and Murray [2, 8] shows that the data obtained by the BRAHMS Collaboration at 200 GeV/A has a clear dependence of the baryon chemical potential on rapidity which is revealed through the changing $\bar{p}/p$ ratio with rapidity. Biedroń and Broniowski [2, 9] have done an analysis of rapidity dependence of the $\bar{p}/p$, K^+/K^-, π^+/π^- ratios based on a single freeze-out model of relativistic nuclear collisions. They have used a single fireball model where the baryon chemical potential depends on the spatial rapidity $\alpha_{||} = \mathrm{arctanh}(z/t)$ inside the fireball. They use single temperature parameter for the entire fireball at the freeze-out (≈ 165 MeV). Their model is very successful in explaining the proton, antiproton and the (anti)Kaon rapidity spectra. They have used a parameterization for the functional dependence of the chemical potentials at low values of $|\alpha_{||}|$ as $\mu = \mu(0)[1 + A\alpha_{||}^{2.4}]$. Here the power is chosen to be 2.4 instead of 2 which according to these authors works better. Fu-Hu Liu *et al.* [10] have recently attempted to describe the transverse momentum spectrum and rapidity distribution of net protons produced in such high energy nuclear collisions by using a new approach *viz.* a two cylinder model [11–13].

2. Model

We briefly discuss the model used here. In order to describe the rapidity distribution of the produced hadrons in ultra-relativistic nuclear collisions, the statistical thermal model has been extended to allow for the chemical potential and temperature to become *rapidity dependent* [5, 9, 14–16]. The thermal model assumes that the rapidity axis is populated with hot regions (fireballs) moving along the beam axis with monotonically increasing rapidity, $y_{\rm FB}$. The emitted particles leave these local regions (fireballs) at the freeze-out following a (local) thermal distribution. The resulting rapidity distribution of any given particle specie j is then obtained by a superposition of the contribution of these regions (fireballs) given by the following equation

$$\frac{dN^j(y)}{dy} = A \int\limits_{-\infty}^{+\infty} \rho(y_{\rm FB}) \frac{dN_1^j(y - y_{\rm FB})}{dy} dy_{\rm FB} \,, \tag{1}$$

where y is the particle's rapidity in the *rest frame* of the colliding nuclei and A is the arbitrary overall normalization factor. The distribution $\frac{dN^j(y)}{dy}$ represents total contribution of all the regions to the jth hadron specie's rapidity spectra. According to the thermal model the rapidity spectra of the hadrons *i.e.* $\frac{dN_1^j(y)}{dy}$ in these local regions (fireballs) can be written as

$$\frac{dN_1^j}{dy} = 2\pi g^j \lambda^j \left[m_0^2 T + \frac{2m_0 T^2}{\cosh y} + \frac{2T^3}{\cosh^2 y} \right] e^{-\beta m_0 \cosh y} \,, \tag{2}$$

where T is the temperature of the fireball. The m_0, g^j and λ^j are the rest mass, spin–isospin degeneracy factor and the fugacity of the jth hadronic specie, respectively. The above formula does not require the inclusion of the collective flow effect because it describes the rapidity spectra of hadrons emitted from a small hadronic fluid volume (element) of the entire hadronic fluid. As discussed above, these elements move along the beam axis with different rapidities and hence the $\frac{dN_1^j(y)}{dy}$ yield obtained from each hadronic fluid element through Eq. (2) is superimposed via Eq. (1) to obtain the net yield $\frac{dN^j(y)}{dy}$. Thus various regions (or fireballs), referred to in the model, can be regarded to be like hadronic fluid elements flowing along the rapidity axis with monotonically increasing rapidities, $y_{\rm FB}$, hence in the (final) net yield $\frac{dN^j(y)}{dy}$ the longitudinal flow effect is taken into account. The contribution of the respective regions (or fireballs) to the final hadronic yields is not assumed to be in the equal proportions. It is rather assumed to follow a Gaussian distribution in the variable $y_{\rm FB}$, centred at zero fireball rapidity ($y_{\rm FB} = 0$)

$$\rho(y_{\rm FB}) = \frac{1}{\sqrt{2\pi}\sigma} \exp\left(\frac{-y_{\rm FB}^2}{2\sigma^2}\right) . \tag{3}$$

The value of σ determines the width of the Gaussian distribution. Furthermore, the experimental data provide a strong evidence that the baryon chemical potential (μ_B) of the successive regions (fireballs) should be dependent on their rapidities ($y_{\rm FB}$). Hence the evaluation of the final hadronic yield requires a superposition of the contributions of these regions (fireballs) whose baryon chemical potential increases with their rapidity. For this purpose a quadratic type dependence is considered [2, 4] so as to make μ_B invariant under the transformation $y_{\rm FB} \to -y_{\rm FB}$

$$\mu_B = a + b\, y_{\rm FB}^2 \,. \tag{4}$$

In the recent works [5, 17] it has been further assumed that the temperature of the successive fireballs along the rapidity axis *decreases* (as the baryon chemical potential increases) according to a chosen parameterization of the following type

$$T = 0.166 - 0.139\, \mu_B^2 - 0.053\, \mu_B^4 \,, \tag{5}$$

where the units are in GeV. This gives a temperature of the mid-rapidity region of the fireball (where $y_{\rm FB} \sim 0$) to be $T = (0.166 - 0.139a^2 - 0.053a^4)$ GeV, while it very slowly decreases as $y_{\rm FB}$ increases [17].

Becattini and Cleymans [2,4] provided a good fit to the net proton flow, pion flow and the ratio $\bar{p}/p$ rapidity density distributions, measured at the highest RHIC energy by the BRAHMS Collaboration. The values of their model parameters were, $a = 23.8$ MeV, $b = 11.2$ MeV and $\sigma = 2.183$, while the temperature T was varied according to the parameterization (5). However, a theoretical fit to the individual proton and antiproton rapidity spectra was not provided. Furthermore, the strange sector data on K^+ and K^- rapidity spectra, as measured by the BRAHMS Collaboration in the same experiment for the same experimental conditions and the ratios $\bar{\Lambda}/\Lambda$ and $\bar{\Xi}/\Xi$ were also not tested. The role of the resonance decay, if any, was not studied.

Therefore, in this paper we have attempted to show that in addition to the net proton flow, pion flow and the ratio $\bar{p}/p$ the extended statistical thermal model discussed above can also very effectively explain the *individual* rapidity spectra of various non-strange and strange hadrons such as the protons, antiprotons, Kaons (K^+), antiKaons (K^-), $\bar{\Lambda}/\Lambda$, and the $\bar{\Xi}/\Xi$. We find that the mid-rapidity data (for $|y| < 1$) available (from STAR) on $\bar{\Lambda}/\Lambda$ and $\bar{\Xi}/\Xi$ are fitted quite well. This can be achieved with single set of model parameters *viz.* a, b, σ and single value of the temperature parameter T chosen for all the regions of the fireballs. The chemical potentials have to be made dependent on the fireball rapidity y_{FB}, a situation which is unavoidable in the model due to the nature of the experimental data.

We have also investigated the contribution of the decay products of the heavy resonances to the proton, antiproton, Kaon and the pion rapidity distribution data. The spectrum of a given decay product of a given parent hadron in the rest frame of the fireball can be written as [18]

$$\frac{d^3n^{\mathrm{decay}}}{d^3p} = \frac{1}{2pE}\left(\frac{m_h}{p^*}\right)\int\limits_{E_-}^{E_+} dE_h E_h \left(\frac{d^3n_h}{d^3p_h}\right) , \tag{6}$$

where the subscript h stands for the decaying (parent) hadron. The two body decay kinematics gives the *product* hadron momentum and energy in the "rest frame of the *decaying hadron*" as

$$p^* = \left(E^{*2} - m^2\right)^{1/2} , \tag{7}$$

$$E^* = \frac{m_h^2 - m_j^2 + m^2}{2m_j} , \tag{8}$$

where m_j indicates the mass of the *other* decay hadron produced along with the first one (under consideration). Thus the limits of integration in the Eq. (6) are

$$E_\pm = \left(\frac{m_h}{m^2}\right)\left(EE^* \pm pp^*\right) . \tag{9}$$

Note that $E(E_h)$ and $p(p_h)$ are, respectively, the product (decaying hadron) energy and momentum in the "rest frame of the *fireball*".

In our analysis we have also applied the criteria of exact strangeness conservation. It is done in such a way that the net strangeness is zero not only on the overall basis but also in every region (fireball) separately, as they maintain different baryon chemical potentials. This is essential, because as the rapidity of these formed regions (fireballs) increases along the rapidity axis, the baryon chemical potential (μ_B) also increases, in accordance with Eq. (4). Hence the required value of the strange chemical potential (μ_{s}) varies accordingly with μ_B for a given value of temperature. Consequently, the value of the strange chemical potential (μ_{s}) will vary with y_{FB}.

3. Results and discussion

In Figs. 1 and 2 we have shown the dN/dy (by the solid circles) for the protons and antiprotons, respectively, measured for the top 5% most central Au + Au collisions at $\sqrt{S_{NN}} = 200$ GeV in the BRAHMS experiment. The errors are both statistical and systematic. The experimental data are symmetrized for the negative values of rapidity [7]. The proton's and antiproton's dN/dy data show a maximum at midrapidity and decrease towards higher rapidities ($y \sim 3$). We have fitted both the spectral shapes in Figs. 1 and 2 simultaneously for $a = 25.5$, $b = 12.7$, $\sigma = 2.1$ and $T = 175.0$ MeV.

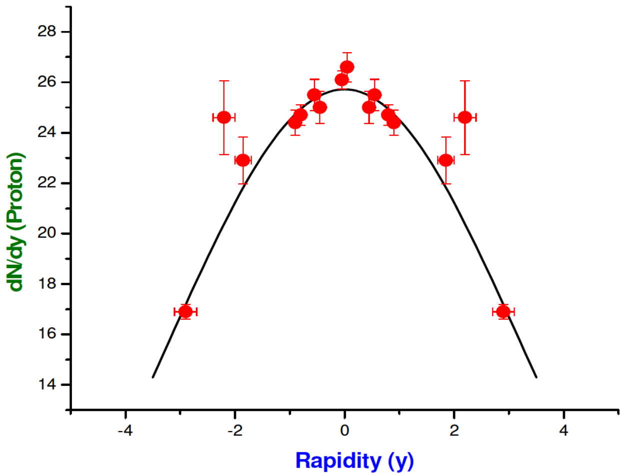

Fig. 1. Proton rapidity spectra. Theoretical result is shown by the solid curve.

We find that the theoretical curves fit the data quite well in both the cases. The theoretical curves also include the contribution of the resonance decays contributions. The minimum (weighted) X^2/DoF for the fitted curve in Fig. 1 is 3.04. We performed an independent fit for proton data first to obtain the model parameters, and then tested it on the antiproton data also and found that it fits well. Corresponding to these model parameters the (weighted) X^2/DoF value of the fitted curve for the antiproton data in Fig. 2 turns out to be 4.81, which is reasonable in view of the relatively small error bars in the antiproton data.

It may be noted that the proton spectra (experimental as well as theoretical) in Fig. 1 is seen to be slightly broader than the antiproton spectra in Fig. 2. This according to the present model can be explained. It emerges from the fact that since $\mu_B \sim y_{\rm FB}^2$ and the rapidity axis is assumed to be populated by the regions (fireballs) of successively increasing rapidity $y_{\rm FB}$ and hence increasing chemical potentials (since $\mu_B = a + b\, y_{\rm FB}^2$), consequently the low rapidity (y) baryons (which have a larger population in a baryon rich

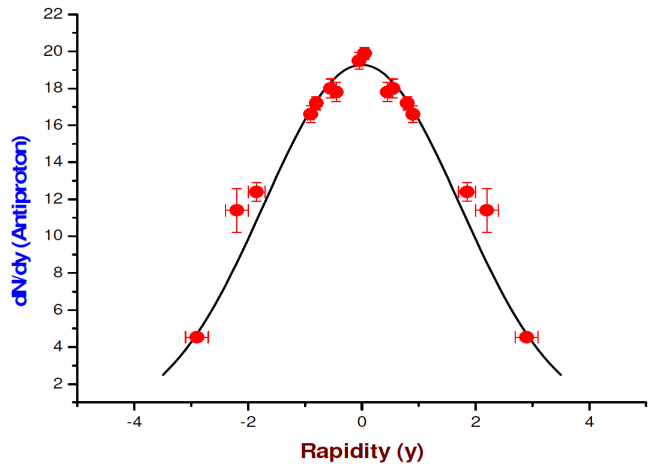

Fig. 2. Antiproton rapidity spectra. Theoretical result is shown by the solid curve.

fireball in thermo-chemical equilibrium) emitted in the forward (backward) direction from a *fast* moving region (fireballs with large $y_{\rm FB}$), appear with a large value of rapidity (y) in the *rest frame of the colliding nuclei*. In other words, as μ_B increase monotonically along the rapidity axis ($\sim y_{\rm FB}^2$) there is an increase in the *density* of protons and a simultaneous suppression in the density of antiprotons thereby making the proton rapidity spectrum broader than that of the antiproton's.

We also compare these theoretical spectral shapes of the dN/dy distributions of protons (antiprotons) with the cases when resonance decay contributions are not taken into account.

In Figs. 3 and 4 we have shown a *pure thermal* (*i.e.* the directly produced) proton's and antiproton's distributions, respectively (*i.e.* excluding the resonance decay contributions, as discussed above) by the upper and lower curves, respectively and the *total* proton's and antiproton's distributions by the lower and upper curves, respectively (*i.e.* including the resonance decays).

To facilitate a proper comparison of the shapes, the two curves have been normalized at $y = 0$ in both the figures, where the units are arbitrary. We notice that the spectral shapes for the case when resonance decay contributions are taken into account are (slightly) narrower than the spectral shape of the protons of the pure thermal origin while for the antiprotons the two are almost same. Hence we find no major change of rapidity spectral shape due to resonance contributions.

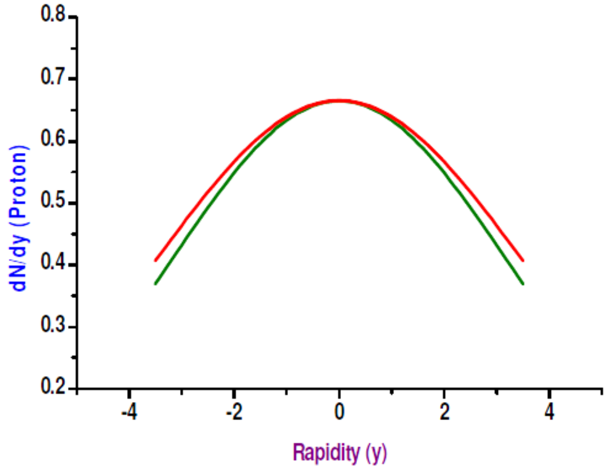

Fig. 3. Rapidity spectra of pure thermal protons (*i.e.* excluding the resonance decay contributions) shown by upper curve and the total protons shown by lower curve (*i.e.* including the resonance decays).

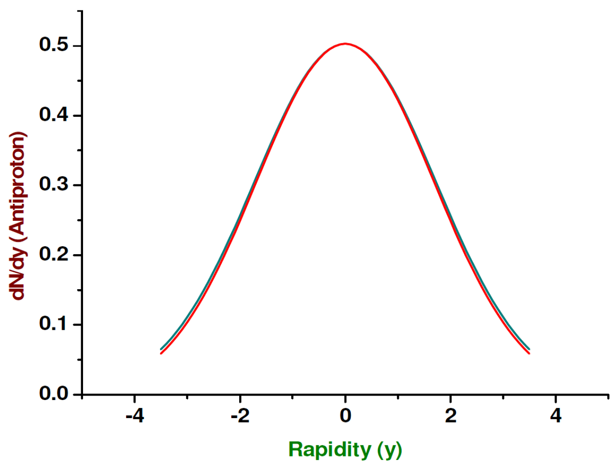

Fig. 4. Rapidity spectra of pure thermal antiprotons (*i.e.* excluding the resonance decay contributions) shown by lower curve and the total antiprotons shown by upper curve (*i.e.* including the resonance decays).

In order to highlight this, we have in Fig. 5 plotted the *ratio* of the two yields (*i.e. total* protons *versus pure thermal* protons) *versus* the rapidity. We find that the ratio is nearly constant between $y = 0$ to $y \approx 3$. The variation in the ratio between these limits of the rapidity variable is $< 6\%$.

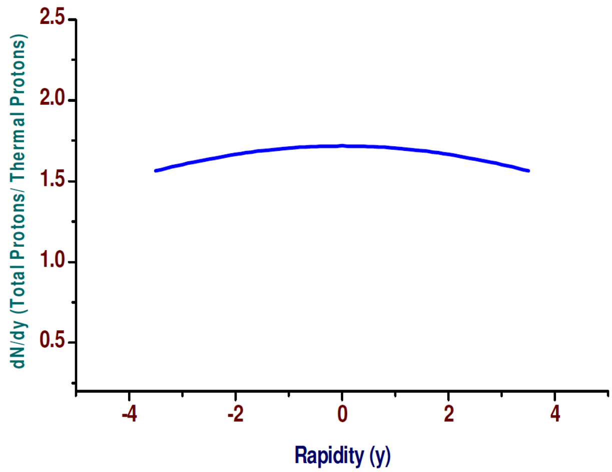

Fig. 5. Ratio of the total protons *versus* pure thermal protons plotted with rapidity.

Furthermore, we also find that the spectral shape of the *product* hadron is very slightly narrower than that of the *parent* hadron's. To realize this we have shown in Fig. 6 the rapidity distribution shapes of the *pure thermal* lambdas and that of the protons obtained through its decay. The two curves are very much similar in shape.

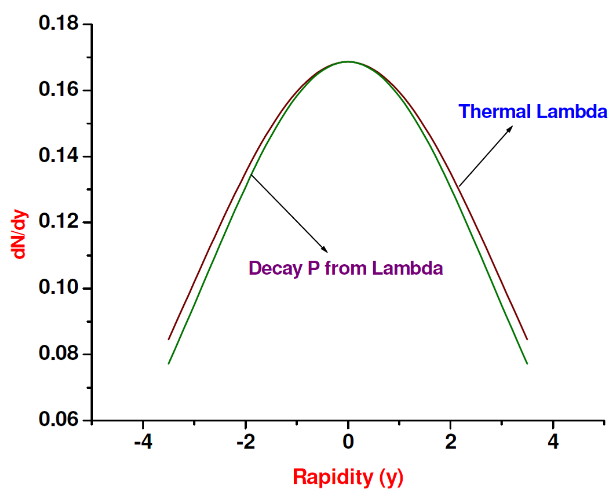

Fig. 6. Rapidity distribution shapes of the pure thermal lambdas and that of the protons obtained through its decay.

In Fig. 7 we have shown the theoretical fit to the net proton flow data. We have also included the recent data points of BRAHMS [7]. The value of the (weighted) X^2/DoF for the fitted curve is 0.19.

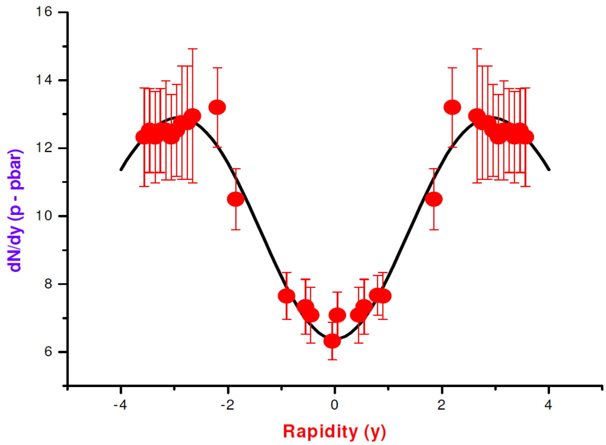

Fig. 7. Rapidity spectra of the net proton flow.

The experimental net proton rapidity distribution data shows a somewhat broad and deep minimum around the mid-rapidity region which is well described by the theoretical solid curve in Fig. 8. This experimental situation is, however, not as earlier has been widely expected [19] that the rapidity distribution of the *net baryons* produced in the ultra-relativistic nuclear collisions will exhibit a very flat and broad minimum measuring several units of rapidity, centred at midrapidity. So far it has not been observed, either in the SPS experiments or even at the highest RHIC energy. The upcoming LHC experiments may throw more light on this aspect and provide a better understanding of the nuclear transparency effect in the ultra-relativistic nuclear collisions.

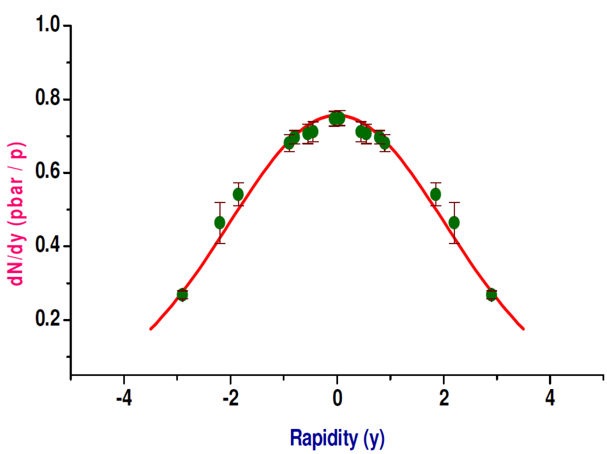

Fig. 8. Rapidity spectra of $\bar{p}/p$ ratio.

The present RHIC experiments at 200 GeV/A, however, have given an indication that these nuclear collisions have begun to show at *least partial transparency*. In Fig. 8 we have shown by the solid curve the rapidity spectra of the $\bar{p}/p$ ratio. The ratio has a somewhat broad maximum (~ 0.75) in the midrapidity region which then decreases to about 25% at around $y \sim 3$. The value of the (weighted) X^2/DoF for the curve is 1.06.

Apart from the analysis of the rapidity spectra of non-strange baryons we have also analyzed the strange meson data as measured by the BRAHMS collaboration at RHIC in the top 5% most central collisions at 200 GeV/A in the same Au + Au collision experiments. We have found that in the above model it is also possible to fully account for the rapidity distributions of Kaons and antiKaons.

In Fig. 9 we have shown the rapidity spectra of Kaon flow. The theoretical curve which fits the data is for the *same* values of the model parameters as used for the theoretical curves in all the previous figures. We find that the theoretical curve provides a very good description of the data. In our calculation we have included the contribution of the decay resonances. Corresponding to these model parameters the (weighted) X^2/DoF value of the fitted curve is 0.70.

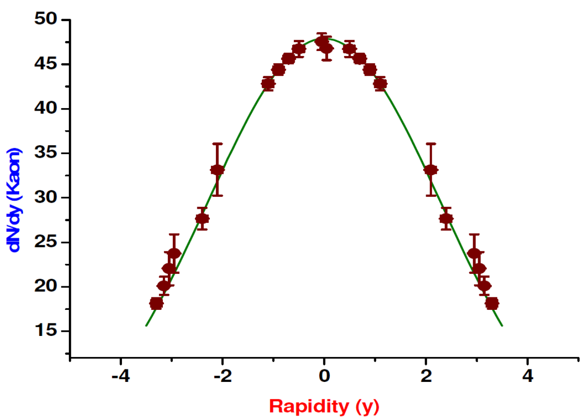

Fig. 9. Rapidity spectra of Kaon flow. The theoretical curve which fits the data is for the same values of the model parameters as used for the other theoretical curves.

Similarly, in Fig. 10 we have shown the rapidity spectra of antiKaons. The theoretical curve which fits the data is again for the same values of the model parameters. The X^2/DoF for the fitted curve is 4.69.

Here again, we find that the Kaon spectra is broader than the antiKaon spectra as is also noticed for the proton spectra which is broader than the antiproton spectra. This is again due to the increasing chemical potential of the successive regions (fireballs) formed along the rapidity axis.

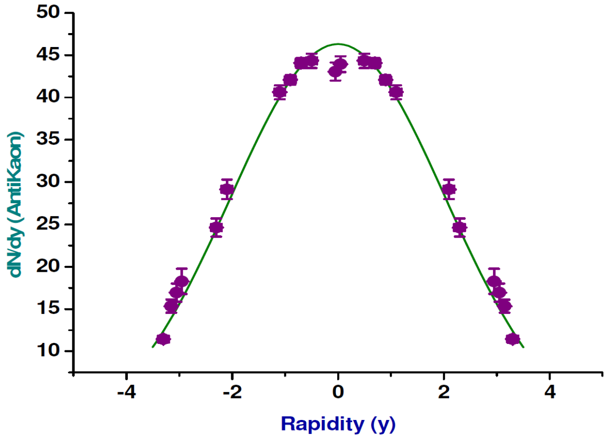

Fig. 10. Rapidity spectra of antiKaon flow. The theoretical curve which fits the data is for the same values of the model parameters as used for the theoretical curves in all previous cases.

When we consider the resonance decay contributions to the spectral shapes of the Kaons and antiKaons, we again find that the spectral shape of the *product* Kaons and antiKaons are almost the same as that of the *parent* hadron's, *i.e.* K^*s. To realize this we have shown in Fig. 11 the rapidity

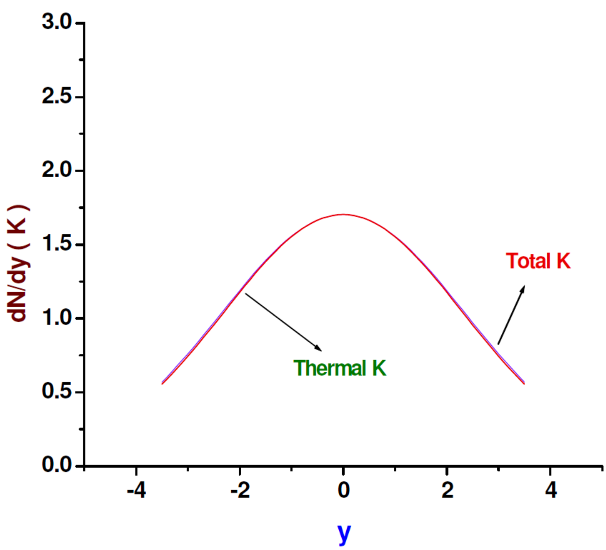

Fig. 11. Rapidity distribution shapes of the pure thermal Kaons and that of the total Kaons which include the contributions of the resonance decays.

distribution shapes of the *pure thermal* Kaons and that of the total Kaons including the resonance decay contributions. The two curves are normalized (at $y = 0$) to facilitate a proper comparison of the shapes. We find that they are similar in shape.

In Fig. 12 we have shown the theoretical rapidity spectra of the ratio $\bar{\Lambda}/\Lambda$.

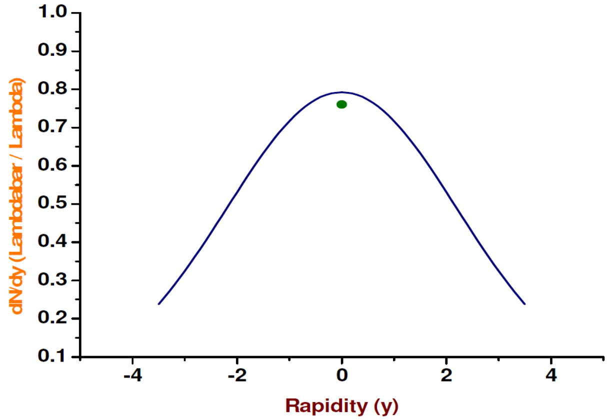

Fig. 12. Rapidity spectra of $\bar{\Lambda}/\Lambda$ flow. The midrapidity data point from the STAR is shown.

The Fig. 13 shows the theoretical rapidity spectra of the ratio $\bar{\Xi}/\Xi$. The mid-rapidity data (for $|y| < 1$) available from STAR [20] fit quite well in both these cases. The theoretical curves are for the same values of the model parameters as the ones used for protons, antiprotons, Kaons and antiKaons.

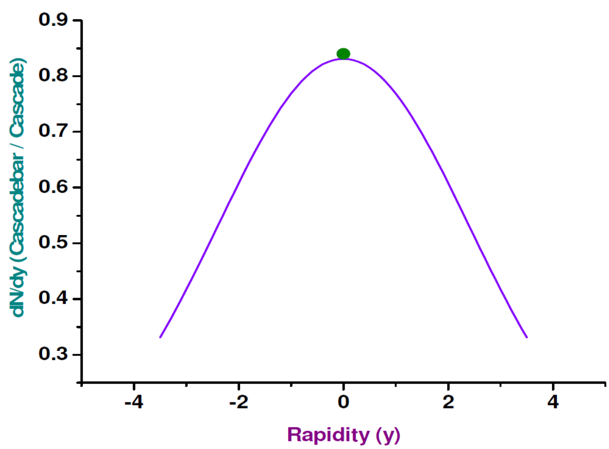

Fig. 13. Rapidity spectra of $\bar{\Xi}/\Xi$ flow.

In Fig. 14 we have shown the theoretical fit to the pion's experimental data. The pion spectrum is also fitted for the *same* values of the model parameters as used in other cases. Corresponding to these model parameters the (weighted) X^2/DoF value of the fitted curve is 6.5, which is somewhat high due to the small error bars in the experimental data.

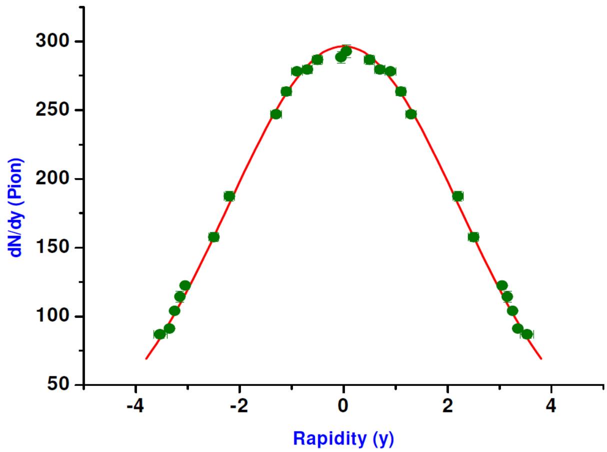

Fig. 14. Rapidity spectra of pion flow. The theoretical result is shown by the solid curve.

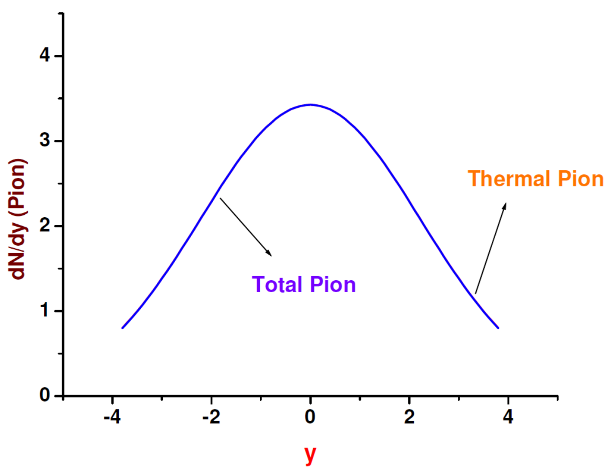

Fig. 15. Rapidity distribution shapes of the pure thermal pions and that of the total pions which include the contributions of the resonance decays of heavier baryonic and mesonic states. The two curves overlap.

In Fig. 15 the rapidity distribution shapes of the *pure thermal* pions and that of the total pions including the resonance decay contributions are shown. As before, the two curves have been normalized to facilitate a proper comparison of the shapes. We again find that the inclusion of the resonance decay contributions leave the rapidity spectral shape almost unchanged.

4. Summary and conclusions

We have used an extended statistical thermal model, where formation of several hot regions (or so-called fireballs) moving with increasing rapidity ($y_{\rm FB}$) along the beam axis is assumed. The final state hadrons are assumed to be emitted from these fireball regions. A Gaussian profile in $y_{\rm FB}$ is used to weigh the contributions of these regions to the final state emitted hadrons population. A quadratic profile in $y_{\rm FB}$ is used to fix the baryon chemical potentials of these regions. We find that it is possible to explain not only the net proton, $\bar{p}/p$ and pion flow but also the individual proton, antiproton, Kaon, antiKaon, $\bar{\Lambda}/\Lambda$ and the $\bar{\Xi}/\Xi$ rapidity. It is interesting to find that the model can successfully explain the strange sector data, measured in the same experiment by the BRAHMS and the STAR Collaboration. This is achieved by using *single* set of the model parameters. We also study the effect of the resonance decay products on the rapidity spectra of the hadrons. We find that the rapidity spectra of the decay products are very slightly narrower than that of the parent hadrons, while the pure thermal rapidity distribution of a given hadronic specie is found to be almost the same as that of the total hadrons, which include the resonance decay contributions.

Jan Shabir is grateful to the University Grants Commission, New Delhi, for the financial assistance during the period of deputation. Waseem Bashir is thankful to the University Grants Commission for providing the Project Fellowship. Saeed Uddin is thankful to the University Grants Commission (UGC), New Delhi, for the Major Research Project grant. Riyaz Ahmad Bhat is grateful to the Jamia Millia Islamia for providing Scholarship. M. Farooq Mir is thankful to the DST, New Delhi for the financial assistance.

REFERENCES

[1] E. Kornas *et al.* [NA 49 Collaboration], *Eur. Phys. J.* **C49**, 293 (2007).

[2] F. Becattini *et al.*, `arXiv:0709.2599v1 [hep-ph]`.

[3] Fu-Hu Liu *et al.*, *Europhys. Lett.* **81**, 22001 (2008).

[4] J. Cleymans, *J. Phys. G* **35**, 1 (2008).

[5] J. Cleymans *et al.*, *Phys. Rev.* **C78**, 017901 (2008) [arXiv:0712.2463v4 [hep-ph]].

[6] G.J. Alner *et al.*, *Z. Phys.* **C33**, 1 (1986).

[7] F. Videbeak, *Nucl. Phys.* **A830**, 43c (2009); I.G. Bearden *et al.* [BRAHMS Collaboration], *Phys. Rev. Lett.* **93**, 102301 (2004).

[8] L.A. Stiles, M. Murray, arXiv:nucl-ex/0601039.

[9] B. Biedroń, W. Broniowski, *Phys. Rev.* **C75**, 054905 (2007).

[10] Fu-Hu Liu *et al.*, *Europhys. Lett.* **81**, 22001 (2008).

[11] Fu-Hu Liu *et al.*, *Phys. Rev.* **C69**, 034905 (2004).

[12] Fu-Hu Liu, *Phys. Rev.* **C66**, 047902 (2002).

[13] Fu-Hu Liu, *Phys. Lett.* **B583**, 68 (2004).

[14] F. Becattini, J. Cleymans, *J. Phys. G* **34**, S959 (2007).

[15] F. Becattini *et al.*, *PoS* **CPOD07**, 012 (2007).

[16] W. Broniowski, B. Biedroń *J. Phys. G* **35**, 044018 (2008) [arXiv:0709.0126 [nucl-th]].

[17] J. Cleymans *et al.*, *Phys. Rev.* **C75**, 034905 (2006).

[18] Saeed Uddin *et al.*, *Int. J. Mod. Phys.* **A21**, 1471 (2006).

[19] J.D. Bjorken, *Phys. Rev.* **D27**, 140 (1983).

[20] J. Adams *et al.*, *Phys. Rev. Lett.* **98**, 062301 (2007).